Effect on Microstructure of Acid-Catalyzed PTMO/TEOS and PTMO/TIOPR Hybrids When Aged in Neutral and Alkaline Aqueous Solutions

Chinmay S. Betrabet and Garth L. Wilkes*

Polymer Materials & Interfaces Laboratory and Department of Chemical Engineering, Virginia Polytechnic Institute and State University, Blacksburg, Virginia 24061-0211

Received September 27, 1994. Revised Manuscript Received January 9, 1995[⊗]

Hybrid networks of functionalized poly(tetramethylene oxide) (PTMO) and tetraethylorthosilicate (TEOS) or titanium isopropoxide (TIOPR) were prepared through the sol–gel route. The films formed by this approach were then immersed in solutions of varying alkalinity for a period of time, removed, and dried overnight under vacuum. This treatment resulted in a better-defined two-phase microstructure in the PTMO/TEOS hybrids because of the solubility of silicon oxide in the highly basic solution. The treated hybrids exhibited higher PTMO chain mobility to the extent that the oligomeric chains could now undergo crystallization at low temperatures. The loss of silicon oxide and hydrolysis of the alkali-treated network resulted in a lower modulus than the untreated hybrid. In the PTMO/TIOPR hybrid, due to the lower solubility of titanium oxide, the base treatment resulted in little change in the titanium oxide content but phase separation between the oligomer and the inorganic oxide was increased which also resulted in a higher mobility of the organic phase. Transmission electron microscopy data qualitatively support these proposed microstructural changes.

Introduction

Over the past two decades interest in sol–gel process has been growing because of its potential to synthesize new materials whose composition and homogeneity can be controlled at the molecular level.[1] The sol–gel reaction generally involves semimetal and metal alkoxide precursors and can be divided into two major steps:[2] the hydrolysis reaction and the condensation reaction. The hydrolysis reaction involves the following reaction:

$$\text{M–OR} + \text{H}_2\text{O} \leftrightarrow \text{M–OH} + \text{ROH} \qquad (1)$$

where M denotes such species as Si, Ti, Zr, etc., and R denotes an organic group, typically a low molecular weight alkyl group. The reaction can be catalyzed using an acid or base catalyst. The condensation reaction can generally be differentiated into two reactions, namely, the water-producing condensation reaction (oxolation) and the alcohol-producing condensation reaction (alcoxolation) as shown below:

$$\text{M–OH} + \text{HO–M} \leftrightarrow \text{M–O–M} + \text{H}_2\text{O}$$

and/or

$$\text{M–OH} + \text{RO–M} \leftrightarrow \text{M–O–M} + \text{ROH} \qquad (2)$$

Both acid and base catalysts can catalyze sol–gel reactions. The reactions are quite complex because of the effect of neighboring groups on the reactivity of the alkoxy and hydroxy species and the effect of reaction conditions such as solvent medium, water concentration, and chemical nature of the alkoxy species.[2,3] Under acidic conditions the hydrolysis reaction is faster than the condensation step, the latter of which then serves as the rate-determining step. In contrast, under basic conditions the hydrolysis step is rate determining. The susceptibility of an alkoxide group to hydrolysis is also affected by the neighboring groups. Acid catalysis occurs at pH's lower than the isoelectric point of the metal oxide species while base catalysis occurs at higher pH. Under acid-catalyzed reactions of multifunctional alkoxides, every subsequent hydrolysis step in a metal alkoxide species is slower than the previous step. Thus in a single metal alkoxide species, not all alkoxide groups are hydrolyzed before the condensation reaction is initiated. It must be noted, however, that the extent of hydrolysis before condensation reactions begin is also dependent on the concentration of the alkoxide in the solution. Generally, under acid catalysis, a more "open" polymer-like network structure is obtained. In contrast to the acid-catalyzed process, under basic conditions, each subsequent hydrolysis step on the metal alkoxide species is faster than the previous step, resulting in compact inorganic particulate species being formed. Thus, the morphology obtained from acid- and base-catalyzed reactions can be quite different as has been discussed in detail elsewhere.[2,3]

The synthesis of hybrid materials where inorganic–organic materials are chemically linked is a relatively new variation on this process. For example, Schmidt and co-workers have demonstrated some useful applications of hybrid materials.[4,5] Mark et al.[6] have infused cross-linked poly(dimethylsiloxane) films with tetra-

* To whom correspondence should be directed.

⊗ Abstract published in *Advance ACS Abstracts,* February 15, 1995.

(1) Yoldas, B. E. *J. Mater. Sci.* **1977,** *12,* 1203–1208.

(2) Brinker, C. J.; Scherer, G. W. *Sol-Gel Science: The Physics and Chemistry of Sol-Gel Processing*; Academic Press: New York, 1990; Chapter 3.

(3) Livage, J.; Henry, M.; Sanchez, C. *Prog. Solid State Chem.* **1988,** *18,* 259–341.

0897-4756/95/2807-0535$09.00/0

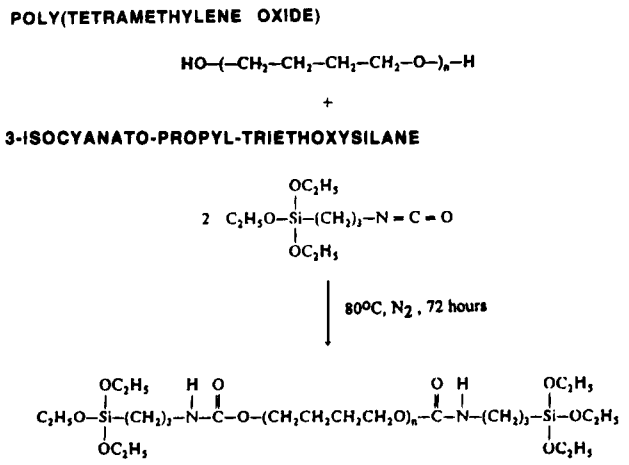

Figure 1. Schematic of endcapping reaction of poly(tetramethylene oxide).

ethylorthosilicate (TEOS) and precipitated silica particles through the sol–gel process. Other workers[7] have investigated the potential of using such hybrid materials in polymeric electrode applications.

Work in our laboratory[8–12] has focused on the preparation and characterization of many different hybrid network materials using alkoxides of titanium, zirconium, aluminum, and silicon with a variety of oligomers such as poly(tetramethylene oxide) (PTMO), poly(dimethylsiloxane), polyimides, poly(ether ketone), and low molecular weight compounds such as diethylenetriamine, melamine and triphenylphosphine oxide. Prior to the preparation of hybrid materials, the oligomer, which generally has amine or hydroxyl endgroups, is end functionalized with a reagent: (3-isocyanatopropyl)-triethoxysilane. A scheme for the endcapping reaction is shown in Figure 1. The details of the endcapping procedure have been provided in previous communications.[10,11]

A scheme for the preparation of acid-catalyzed hybrid materials using TEOS has been given elsewhere.[10,11] These materials have been prepared typically by mixing the functionalized oligomer and the inorganic metal alkoxide together with water and catalyst (acid) in a suitable solvent. After a minute of mixing, the homogeneous mixture is poured into polystyrene dishes. After 7 days, the films formed after gelation and solvent evaporation are peeled from the dishes and characterized. Other procedures for obtaining hybrid materials have been to use microwave curing;[10] prehydrolyzing the metal alkoxide;[11] and casting films at higher temperatures rather than at ambient temperatures.[12]

On the basis of some of the results obtained from the study of acid-catalyzed hybrid materials, Huang et al.[13] proposed a general morphological model for the microstructure of the hybrid materials in which the inorganic

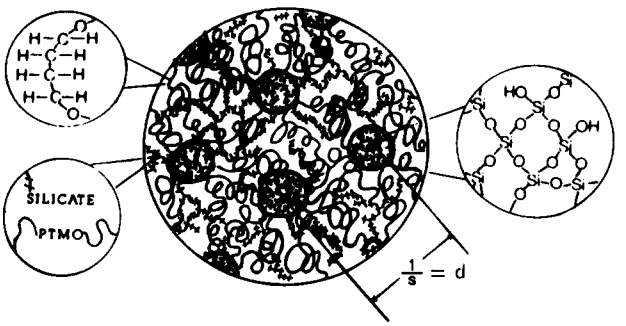

Figure 2. Schematic of the generalized morphological model for ceramers; from ref 9.

phase is assumed to be the dispersed phase as shown in Figure 2. The model shows oligomeric rich matrix in which silicon oxide species are dispersed. Embedded within this matrix are regions (domains) where the silicon oxide concentrations are much higher than the surrounding matrix. These domains are partially periodically arranged with a general spacing of ca. 100 Å as denoted by d in Figure 2. The authors hypothesized that the mobility of the oligomeric chains is retarded by encapsulation of some of the chains by the relatively rigid silicon oxide phase in the matrix and the chain ends by the silicon oxide domains. Further considerations of this model have been recently addressed by Rodrigues and Wilkes.[14]

The reaction of multifunctional alkoxides to form metal oxides inevitably leads to a cross-linked network. If the extent of reaction is sufficiently high, the reactant mixture gels, and the reaction mixture is unable to flow. Gelation can be thought of as a gross reduction in mobility, due to the onset of an infinite network being established. At the microlevel or over smaller length scales, however, it has been observed that in some systems the molecular mobility may be sufficient to be able to continue with the condensation reactions. With respect to this paper, *a key point to note is that all processes that occur after gelation are collectively denoted as **aging** processes*. The same polymerization reactions that constitute the sol–gel reaction, viz., hydrolysis and condensation, side reactions, and the reverse reactions may also occur during aging, although at a much slower rate because of the lower mobility of the reactive groups. In addition, the localized dissolution and reorganization of the inorganic gel in the aging solution also influences the structure of the final product.

The solvent also plays a major role in influencing the course of the aging process and ultimately the final structure. For example, water may play an important role in aging, partly because of its status as a reactant in the sol–gel reaction and partly because it can act as a solvent. As will be shown below, silica is quite soluble in water under sufficiently alkaline conditions, while titanium oxide, found in titania-based hybrids (TIOPR/PTMO), is not. The hydrous titania that is formed under aqueous conditions is known to be amphoteric and has a composition of $TiO_2 \cdot 2H_2O$. Hydrous titania has been found to be insoluble in dilute alkali solutions although it can be solubilized in concentrated alkali metal hydroxide solutions and mineral acids.[15–17] In

(4) Schmidt, H.; Walter, H. *J. Non-Cryst. Solids* **1990**, *121*, 428.
(5) Philipp, N.; Schmidt, H. *J. Non.-Cryst. Solids.* **1984**, *63*, 282.
(6) Sur, G. S.; Mark, J. E. *Eur. Polym. J.* **1989**, *21* (2), 1051.
(7) Ravaine, D.; Seminel, A.; Charbouillot, Y.; Vincens, M. *J. Non-Cryst. Solids* **1986**, *82*, 210.
(8) Rodrigues, D. E.; Brennan, A. B.; Betrabet, C.; Wang, B.; Wilkes, G. L. *Chem. Mater.* **1992**, *4*, 1437–1446, and references therein.
(9) Huang, H.; Orler, B.; Wilkes, G. L. *Polym. Bull.* **1985**, *14*, 557.
(10) Rodriques, D. E.; Wilkes, G. L. *Am. Chem. Soc., Div. Polym. Chem.* **1989**, *30* (2), 227.
(11) Wang, B.; Brennan, A. B.; Huang, H.; Wilkes, G. L. *J. Macromol. Sci.–Chem.* **1990**, *A27* (12), 1449.
(12) Huang, H.; Orler, B.; Wilkes, G. L. *Macromolecules* **1987**, *20* (6), 1322.
(13) Huang, H.; Glasser, R.; Wilkes, G. L. *Inorganic and Organometallic Polymers*; Zeldin, M., Wynne, K. J., Allcock, H. R., Eds.; ACS Symposium Series 360, 1987; p 354.
(14) Rodrigues, D. E.; Wilkes, G. L. *J. Inorg. Organomet. Polym.* **1993**, *3*, 197.

contrast, silica can react with water to form soluble silicic acid:[2]

$$SiO_2 + 2H_2O(l) \leftrightarrow H_4SiO_4 \quad (3)$$

The solubility of silica in aqueous solutions has been extensively discussed by Iler.[18] Below pH 9, the solubility of silica is nearly independent of pH. Above pH 9, the increase in solubility is due to the increased ionization of the silicic acid. The silicic acid is deprotonated leaving a negative charge to stabilize the complex against precipitation:

$$H_4SiO_4 \leftrightarrow H_3SiO_4^- + H^+ \quad (4)$$

As a result of this reaction the silica solubility increases dramatically above pH 9. Below pH 7 the silicic acid is weakly ionized. The solubility of amorphous silica is low in pure water and ranges from 80 to 130 ppm. At pH 7 only 0.2% of the dissolved silica is dissociated, but at pH 12 the concentration of dissociated silica is greater than 90%.[18] The soluble silica is present as a distribution of species.[19,20] Glasser and Lachowski[19,20] studied the composition of sodium silicate aqueous solutions as a function of pH. At a pH of 12.5, cyclic oligomers of up to eight silicon atoms (Si_8) were detected and the cyclics Si_6 through Si_8 were at their maximum concentrations. As the pH decreased, the concentrations of monosilicate through Si_4 decreased. The solution gelled at pH 10.5, where the only species detected was the monosilicate species. Aged silica solutions contained little monomer, a trace of dimer, and polysilicate species, indicating that most of the silica was in a polymerized state. The polymerized species were not chainlike and tended to form globular clusters and cagelike structures which were highly condensed. The groups at the surface served as the reactive points for future growth.

The solubility of silica in organic solvents is low. Iler[18] has shown that the solubility of silica decreases from 140 mg/L at pH 9.5 in water, to 5 mg/L in 90 wt % methanol–water mixture.

In view of the differences in solubility behavior of silica and titania under alkaline conditions and due to the fact that some rearrangement in their structure is possible in specific chemical environments, one objective of this work was to observe the effect of utilizing this approach in modifying the morphological features of some of our earlier prepared hybrid materials. Specifically, two different hybrid networks were prepared and investigated, one based on PTMO and TEOS and the other based on PTMO and TIOPR. Each of these systems was comparable in terms of the initial weight of the metal alkoxide as will be discussed below. While there is some difference in reactivity of the TEOS with respect to that of the TIOPR, there is also, as discussed above, the great difference in the solubility of the silicon oxide versus titanium oxide in the alkaline environment. A similar approach has been taken by Brennan and co-workers,[21] who investigated the effect of triethyleneamine solutions on the structure of PTMO/TEOS hybrids.

Since it is expected that silicon oxide will dissolve to a large extent under basic conditions, another objective of this study was to examine the underlying morphology of the PTMO/TEOS system after the silicon oxide was solubilized. This was done to clarify some of the assumptions regarding encapsulation of PTMO chains made by Huang[13] in developing the earlier microphase morphological model for the PTMO/TEOS hybrid materials; recall Figure 2.

Table 1. Various Treatments Given to Hybrid Materials and Their Designations

sample	aging solution, immersion time	sample designation
PTMO/TEOS	none	sample A
PTMO/TEOS	1 M NaOH, 1 day	sample B1
PTMO/TEOS	1 M NaOH, 2 days	sample B2
PTMO/TEOS	1 M NaOH, 4 days	sample B3
PTMO/TEOS	water, 8 days	sample C
PTMO/TEOS	0.1 M NaOH, 1 day	sample D
PTMO/TEOS	excess of NaOH in IPA, 1 day	sample E
PTMO/TEOS	3.3% (wt/wt) triethylamine in IPA, 1 day	sample F
PTMO/TIOPR	none	sample G
PTMO/TIOPR	1 M NaOH, 1 day	sample H

Experimental Section

Hybrid Film Preparation. The hydroxyl-group-endcapped PTMO was first functionalized with (3-isocyanatopropyl)triethoxysilane. A film of the PTMO/TEOS hybrid material was formed through acid catalysis by the standard route as reported earlier.[9,11,12] This involved mixing the functionalized PTMO and TEOS in 2-propanol in the weight ratio 1:1:1 (for the TEOS(50) film), to which was added water and HCl in the molar ratio of 1 mol of alkoxide:1 mol of water:0.018 mol of HCl. The mixture was stirred for 30 s before being poured into polystyrene dishes which were covered. Clear films of the hybrid material were obtained in 5–7 days. The thickness of the films was between 5 and 10 mils. The films were stored in glassine paper pouches under ambient conditions until tested. Testing was usually completed within 2 weeks after the films were formed. These films were denoted as sample A. In the second step the film was immersed in the aging solution for a variable period as will be described in Table 1 (denoted as sample B1 through sample H). After this two-step procedure, the film was allowed to dry overnight under vacuum. Table 1 describes the various aging solutions used and the respective sample designations of the films obtained after treatment in these aging solutions.

Due to the high reactivity of TIOPR, the acid catalyzed PTMO/TIOPR films (sample G) were made by a modified acid-catalyzed procedure. The HCl and the water were first diluted with 2-propanol and then added to the PTMO/TIOPR mixture to prevent a high local concentration of either reactant. The films obtained from the acid-catalyzed step were transparent and had a yellowish tinge which was imparted by the TIOPR. The TIOPR in the hybrid film was present in the proportion (by weight) of 1 part TIOPR:1 part endcapped PTMO. The remaining procedure was similar to the PTMO/TEOS procedure given above.

Characterization. *Stress–Strain Measurements.* Dog-bone specimens measuring 10 mm × 2.9 mm were cut from the cast films. Both ends of the specimen were then sandwiched between masking tape. Stress-strain measurements were undertaken on an Instron 1122 tensile testing machine at a crosshead speed of 2 mm / min. The data were collected directly into a computer which was interfaced with the output of the tensile machine. The data were recorded as a plot of

(15) Whitehead, J. *Kirk-Othmer Encycl. Chem. Tech.*, 3rd ed.; Mark, H., Ed.; Wiley: New York, 1978; Vol. 3, pp 138–139.
(16) Cotton, F. A.; Wilkinson, G. *Basic Inorganic Chemistry*; Wiley: New York, 1976; pp 385.
(17) Burns, D. T.; Townshend, A.; Carter, A. H. *Inorganic Reaction Chemistry*; 2, Part B, Ellis Horwood: Chickester, UK, 1981; p 464.
(18) Iler, R. K. *The Colloidal Chemistry of Silica*; Wiley: New York, 1979.
(19) Glasser, L. S. D.; Lachowski, E. E. *J. Chem. Soc., Dalton Trans. Inorg. Chem.* **1980**, *3*, 393.
(20) In ref 19, p 399.
(21) Miller, T. M.; Brennan, A. B. *ACS Polym. Prepr.* **1993**, *34* (1), 641.

engineering stress vs strain. Three to five replicates were recorded but the data reported shows the results for a single specimen which best represents the average for the sample population. The initial Young's modulus was calculated from the portion of the curve in the initial deformation region (2–5%).

Dynamic Mechanical Analysis. Dynamic mechanical analysis measurements were performed partly on a computer-controlled DDV-IIc Rheovibron dynamic viscoelastometer in the tensile mode. Typical specimen sizes were 3 mm × 30 mm × 0.2 mm. Measurements of the complex modulus as a function of temperature were performed at a heating rate of 1.5 °C/min, over the temperature range −150 to −180 °C at frequencies of 1.1, 11, and 110 Hz. Only the 11 Hz data were reported. The sample chamber was purged with dry nitrogen gas during the run.

Thermogravimetric Analysis. Thermogravimetric data were obtained from a SEIKO 210 TG/DTA instrument. Initial sample weights were approximately 15 mg. The heating rate was 10 °C/min over a range of temperatures from ambient to 750 °C. A nitrogen gas purge of 50 mL/min was used to maintain a nonreactive atmosphere.

Differential Scanning Calorimetry. DSC data were obtained from a SEIKO Model 210 in the temperature range −150 to 200 °C. The heating rate was 20 °C/min unless otherwise specified.

Small-Angle X-ray Scattering. SAXS measurements were performed on a Siemens-Kratky camera. The scattering intensity was determined with a Braun position-sensitive detector from Innovative Technologies Inc. The X-ray beam was generated by a Siemens Cu–W X-ray tube with a voltage generated by a Phillips Model 1726 generator. The raw data were adjusted for temperature, thickness of the sample, parasitic scattering and standardized with respect to a Lupolen polyethylene sample.

Fourier-Transform Infrared Spectra. FTIR spectra were obtained with a Nicolet Model 5DXB spectrometer. A drop of the mixture was placed between KBr plates and then placed in the path of the infrared beam. Typically 32 scans gave a sufficient signal-to-noise ratio.

NMR Spectroscopy. ^{29}Si NMR spectra were obtained on a Bruker MSL-300 solid-state spectrometer operating at 300 MHz. The samples were spun at 3 to 4 kilohertz at the magic angle. Proton decoupling was applied during data acquisition. A delay time of 45 seconds was used between pulses. Two- to four-hundred scans were collected for each sample and fourier transformed using a line broadening of between 50 to 100 Hz.

Transmission Electron Microscopy. TEM specimens of the hybrid materials were prepared using a Reichert UltracutE cryoultramicrotome and were observed under a Philips 420T scanning transmission electron microscope (STEM) at 100 kV.

Results and Discussion

PTMOS/TEOS Materials. Most of the characterization of the films were performed on samples that were immersed in 1 M NaOH for 24 h and dried overnight under vacuum (sample B1). Approximately 0.5 g of the film was immersed in 30 mL of the 1 M NaOH solution prepared using deionized water. Figure 3 shows the SAXS profile of samples A and B1. The figure also shows the SAXS profile of sample C which will be discussed later. Comparing samples A and B1, both profiles exhibit a first-order interference peak at an s value of ca. 0.1 nm^{-1}. The angular variable s is defined as $s = 2 \sin \theta/\lambda$ where θ is half of the radial scattering angle and λ is the wavelength of the X-ray (1.54 Å). The data can best be explained by the microstructural model of the hybrid material proposed by Huang.[13] The first-order interference peak in the SAXS profile is caused by the short-range periodicity of the domains (the domains being the silicate-rich regions in the microstructural model). For sample A, a maximum in the angular intensity, although broad, suggests a microphase-separated system with a partially periodic structure, as expected based on our earlier publications addressing similar structures.[8] The interdomain spacing can be estimated by taking the inverse of the magnitude of s at the peak position and corresponds to an estimated interdomain spacing of ca. 10 nm. Sample B1 also shows a peak implying that treatment with base has not affected the general periodicity of the domains and that the interdomain spacing is still ca. 10 nm, and it is clear that the angular dependance is distinctly related to that from sample A.

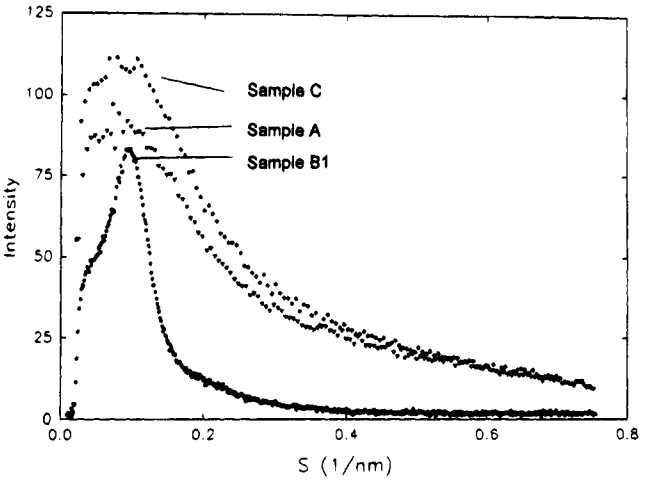

Figure 3. SAXS profiles of samples A, B1, and C.

Sample A shows a gradual decrease in intensity at higher s values in contrast to sample B1 which shows a sharp decrease in intensity beyond the interference peak. The significance of the difference in intensities at the higher s values can be explained, by using as a basis, the earlier microstructural model in Figure 2. Referring to sample A, the contribution to the intensity at higher values of s is also due to fluctuations in electron density but which occur over distances smaller than the interdomain spacing. The inverse relationship between the scattering vector and physical distance is typical of all scattering experiments. A substantial cause of the fluctuation is the variation in the silicon oxide concentration in the matrix and within the silicon oxide domains themselves. The fluctuation is over smaller length scales and so the contribution to intensity from these fluctuations occur at higher values of s. If the silicon oxide were to be distributed homogeneously in the matrix and if the silicate domains were homogenized or fully and uniformly densified, there would be lesser contribution to the intensity at the higher s values, i.e., s values to the right of the interference peak. Sample B1 shows a sharper interference peak of lower intensity and very low intensity at the higher s values which might suggest that the matrix is now more homogeneous and the silicon oxide domains are more densified or at least uniform over the smaller length scale. Homogeneity in electron density over the smaller length scales, in principle, could be achieved by redistribution of the silicon oxide in the matrix to equalize the electron density or by removing the silicon oxide completely from the matrix, in effect segregating the hybrid material into dense silicon oxide domains and the oligomeric network. As will be seen later, homogeneity over smaller length scales occurs by removal of much of the silicon oxide from the matrix.

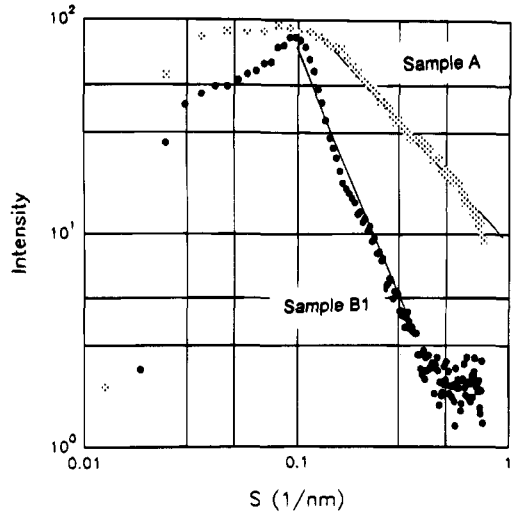

Figure 4. SAXS profiles of sample A and B1 on a double logarithmic scale.

Figure 3 has been replotted on a log–log scale as shown in Figure 4. A plot of this nature, called a Porod plot, can often give an indication of the fractal nature of the silicate domains,[22] specifically if the system displays a mass or surface fractal behavior. This information can be obtained from the region where the intensity decreases linearly with increasing scattering angle. This linear region is called the Porod region and the slope obtained is called the Porod slope. The fractal dimension for our purposes can be used as a measure of the openness of the inorganic domains for mass fractals and a measure of roughness of the surface for surface fractals. A fractal dimension relates the volume of space influenced by the object to its mass or, in the case of fractally rough surfaces, to its surface area. To clarify this description, the volume of any object is related to a characteristic length. By definition, a particle characterized as a *mass fractal* of dimension x implies that the mass of the particle $\propto$ (characteristic length)^x, and a *surface fractal* dimension y is defined by surface area $\propto$ (characteristic length)^y.[22] The fractal dimension of a mass fractal will always be less than the dimensionality of the particle, which implies that the pervading volume of a mass fractal object increases faster than its mass or that its density decreases with increasing volume. An increase in the fractal dimension would imply an increase in the bulk density of the inorganic domains. Fractal dimensions can often be obtained by SAXS measurements if the self-similarity (dilation symmetry) occurs over length scales which are comparable to the length scales probed by X-rays. The slope of the curve in the Porod region, if linear, is a measure of the fractal dimension of the inorganic domains. Objects considered as mass fractals in three-dimensions have fractal dimensions (d_f) ranging from $0 \leq d_f < 3$ with respective Prorod slopes (P) ranging from -3 to 0. Surface fractal objects have fractal dimensions (d_s) ranging from $2 \leq d_s \leq 3$ with Porod slopes ranging from -3 to -4.[22] From mass fractals the Porod slopes are related to the fractal dimension by the formula $P = -d_f$ and for surface fractals $P = d_s - 6$. As mentioned earlier, the slope of the intensity vs s curve in the Porod or power law region can provide this information if indeed linear behavior is observed. Generally, the linear region should extend over a decade to make the analysis more valid. Returning to Figure 4 and comparing sample A with sample B1, it is observed that the slope of sample B1 is much steeper than sample A. Also, unlike sample A, sample B1 exhibits two distinct slopes with a change in slopes occurring at ca. 0.2 mm^{-1} which corresponds approximately to the position of a weak second-order peak. This arguably weak second-order peak may also be barely noted in Figure 4. A correction has to be incorporated for the slope because the SAXS intensity data has been obtained from a slit source rather than a pinhole source.[22] The Porod slope (P) can be obtained from the actual slope by the formula P = actual slope -1. The figure shows that the Porod slope for sample A is -2.07 which implies a mass fractal under acid-catalyzed conditions. In contrast, an unequivocal value for sample B1 cannot be determined because of the presence of the weak second-order peak.[24] As stated above, for determination of fractal dimensions, a constant slope over approximately a length scale of one decade is desired. An average value of -3.7 for the slope for sample B1 can be obtained by combining both slopes which, at least, strongly suggests a surface fractal. In both plots it is recognized that the presence of an interference peak close to the Porod region may influence the exact magnitude of the Porod slope. Nonetheless the figure *clearly shows an increase* in the steepness of the slope *after immersion* in the 1 M NaOH which suggests that the inorganic domains have densified.

Returning to Figure 3, and the profile of sample C, which results from the effect of soaking for 8 days in only deionized water leads to an increase of the intensity of the peak. The general shape of the curve is identical to sample A, but the intensity increase suggests that there has been an increase in the electron density difference between the inorganic phase and the PTMO matrix. This increase is attributed to a higher extent of reaction due to the excess water present in the system. The condensation processes further densify the inorganic phase by removing lower electron density materials such as the organics (alcohols), leaving an increased concentration of the silica in the domains. Brennan also observed an increase in the SAXS peak intensity on immersing hybrid samples of PTMO/TEOS to a 70% (wt/wt) solution of ethylamine in water.[21] In sample C, the peaks have not sharpened, which indicates that as in sample A, a broad distribution of interdomain spacings and/or particle size distribution. It may be recalled that the solubility of silica in aqueous solutions in the region of pH 7 is very low.[18] Thus the rate of dissolution of any of the gelled silicate structure must be slow. A likely mechanism for the densification is that there is condensation of the silanol groups in proximity to each other without large-scale migration of silica over larger length scales.[25] Hence the shape of the SAXS curve generally is unchanged.

Figure 5 shows the SAXS profiles of samples B1 (soaked in 1 M NaOH for 1 day), B2 (1 M NaOH, 2 days), and B3 (1 M NaOH, 4 days). The figure shows

(22) Keefer, K. D. *Better Ceramics through Chemistry II*; Brinker, C. J., Clark, D. E., Ulrich, D. R., Eds.; Mat. Res. Soc.: Pittsburgh, 1986; pp 295–304.
(23) Schaefer, D. W.; Keefer, K. D. *Better Ceramics through Chemistry II*; Brinker, C. J., Clark, D. E., Ulrich, D. R., Mat. Res. Soc.: Pittsburgh, 1986; pp 277–288.
(24) Scherer, G. W. *J. Non.-Cryst. Solids* **1986**, *87*, 199–225.
(25) Rodrigues, D. E.; Wilkes, G. L. *J. Inorg. Organomet. Polym.* **1993**, *3*, 3.

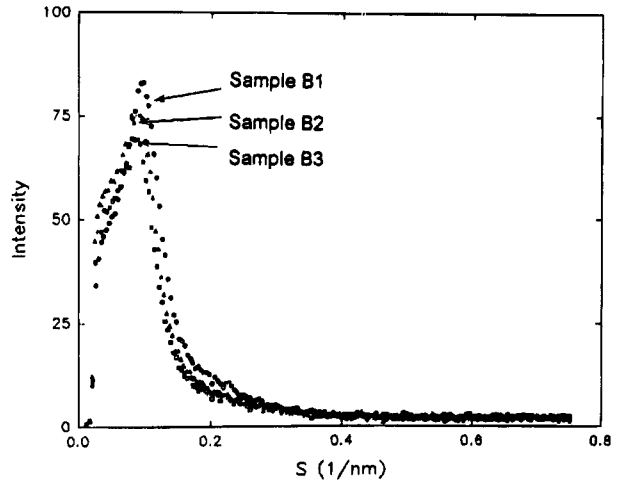

Figure 5. SAXS profiles of samples B1, B2, and B3.

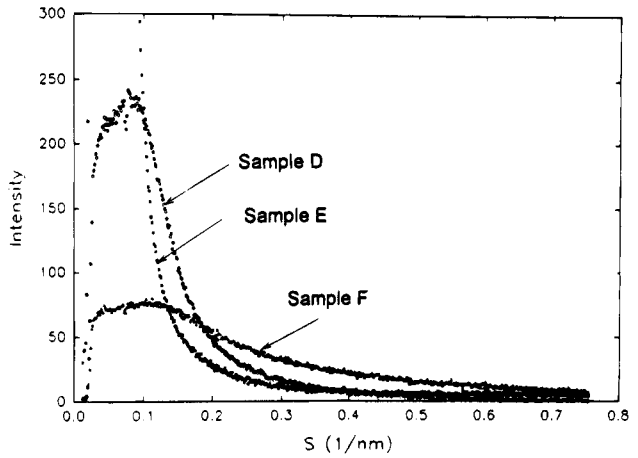

Figure 6. SAXS profiles of samples D, E, and F.

no major changes in the profiles as a function of soaking time. This suggests that residual silica, if present, dissolves slowly with immersion time, hinting that the residual silica bound to the inorganic domains is very tightly bound. Figure 6 shows the effect of various aging solutions on the SAXS profile of the initial hybrid network material. The shape of the profile obtained from sample D (0.1 M NaOH solution for 24 h) is similar to that obtained from sample A in Figure 3, but the intensity is higher, which suggests that densification has increased but the solubility is not sufficient to dissolve the silica domains. This implies that the hydroxyl ion concentration does indeed affect the rate of dissolution of the silica domains, a result which has been observed by Iler.[18] However, sample E soaked in a sodium hydroxide saturated solution of 2-propanol and then dried exhibits a quite different morphology. The original peak *disappears* which indicates that the structural periodicity is absent. The original morphology is now replaced with a *more homogeneous morphology* where the silicate is dispersed more randomly within the PTMO phase. The high intensity of the SAXS profile as gauged by the area under the curve is an indication that most of the silica has not dissolved but remains in the system (as will be shown later), which causes large fluctuations in the electron density. The dissolution is limited by the low solubility of the silica in 2-propanol an inference drawn from Iler's observation of the low solubility of silica in methanol.[18] The low solubility forces the silica to be reprecipitated into the PTMO phase. This more uniform reprecipitation is seen as a "peakless" profile under SAXS. The dried film was indeed brittle, which prevented stress–strain characterization. Treatment with a weak base such as triethylamine in IPA (sample F) was unable to change the morphology or densify the material, i.e., the shape of the SAXS profile was unchanged.

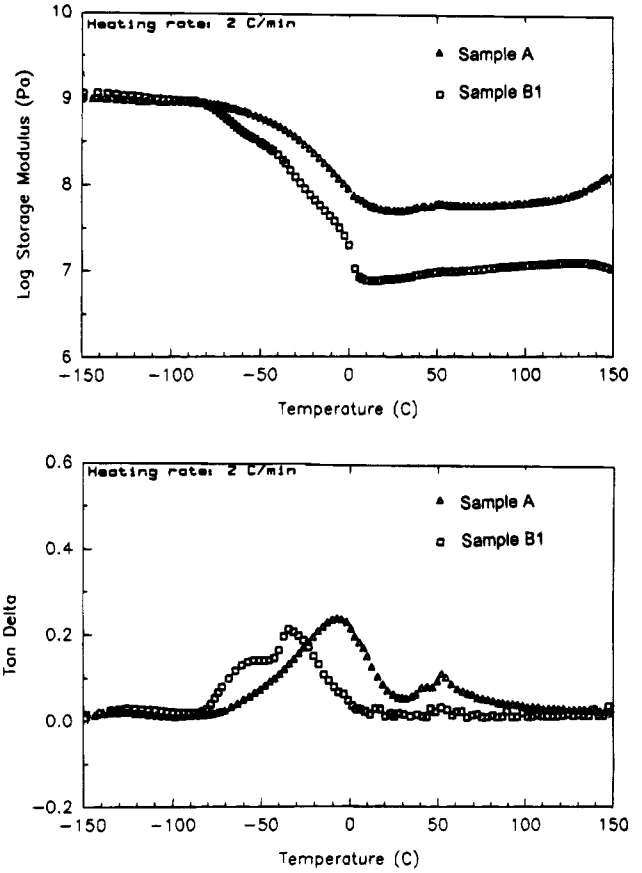

Figure 7. (A) Storage modulus plots of sample A and B1. (B) tan δ plots of sample A and B1.

Figure 7A shows the storage modulus data of samples A and B1. At low temperatures the oligomeric phase is in a glassy state. The onset of the glass transition for the PTMO component is at ca. −80 °C. The glass transition is spread over a wide temperature range signifying a spectrum of environments around the PTMO chain segments. The storage modulus at room temperature and above has a magnitude of 10^7–10^8 Pa, more typical of a polymer above its glass transition temperature which is partially filled and/or cross-linked. For sample B1, the glassy region exhibits no significant difference from sample A, but at the glass transition, a two-step transition is noticed and the modulus at room temperature and above is lower by almost an order of magnitude than sample A. The tan δ plots of sample A and B1 also make the two steps apparent. Figure 7B shows the tan δ plots of samples A and B1 as a function of temperature. The small peak in the tan δ spectrum at approximately −130 °C is attributable to the well-known crankshaft motion of the methylene units of the PTMO chain.[26] Sample A shows a broad glass transition peak which again is characteristic of oligomeric chains having a variety of environments. The glassy region for sample B1 exhibits no significant difference from sample A, but the glass transition is now decreased as noted from the lower tan δ peak temperature. This

(26) Schatzki, T. F. *J. Polym. Sci.* **1962**, *57*, 496.

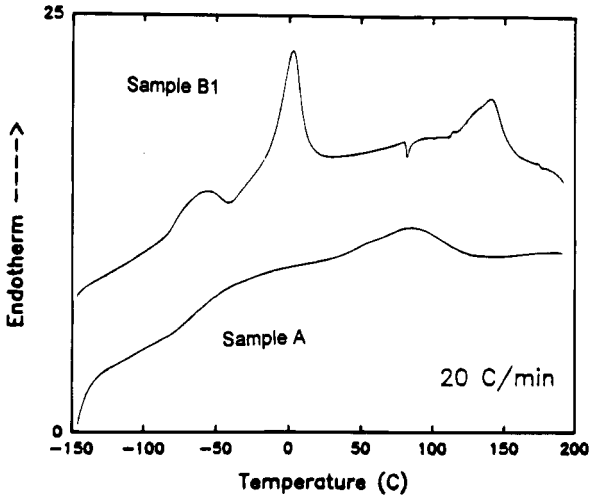

Figure 8. DSC scans of samples A and B1.

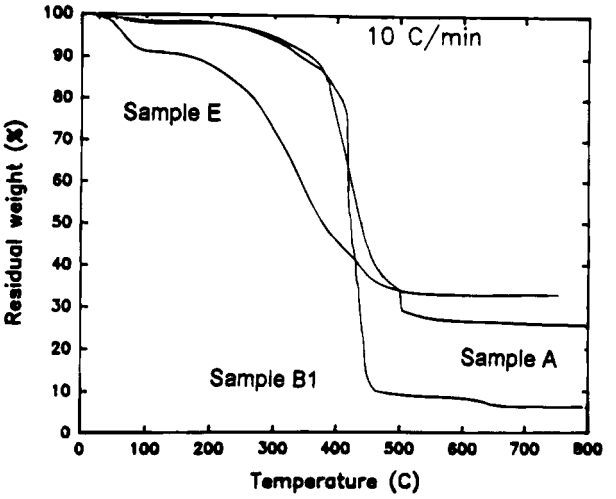

Figure 9. TGA profiles of samples A, B1 and E.

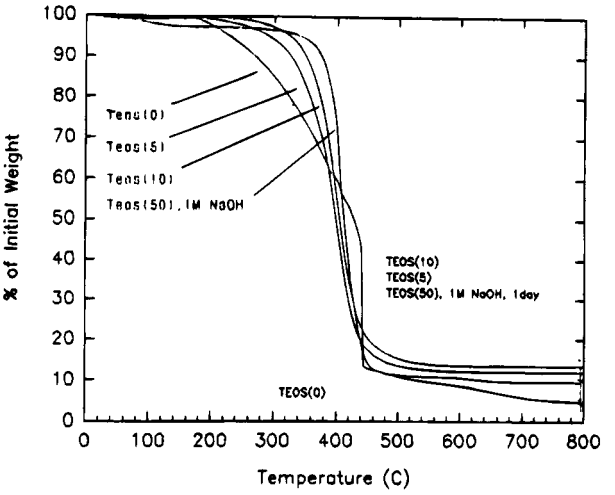

Figure 10. TGA profiles of TEOS–PTMO hybrids.

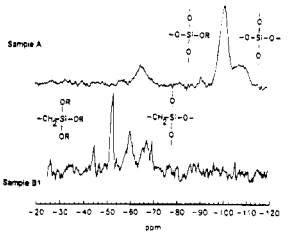

Figure 11. ^{29}Si solid-state MAS NMR spectra of samples A and B1.

shift to lower temperatures suggests that the oligomeric chains are less constrained and hence relax at lower temperatures. The new peak in the tan δ spectrum is at ca. −35 °C and is attributed to the crystallization of the PTMO chains. Evidence that the second peak was due to crystallization of the PTMO was confirmed by DSC experiments (Figure 8). For this latter analysis, each sample was held at −60 °C in the calorimeter. Thereafter the samples were cooled to below the glass transition temperature, and data were collected during the heating stage of the run. The acid-catalyzed sample (sample A) exhibited no melting peak beyond the T_g in contrast to the 1 M NaOH treated sample (sample B1) that exhibited a distinct exothermic peak just beyond the T_g, which corresponds to a crystallization of the PTMO chains, and an endothermic peak corresponding to the melting of the crystallites on further heating. Certainly some crystallization may have occurred during the cooling of the sample which explains the unequal areas of the endotherm and the exotherm. It is thus concluded that treatment with base has the effect of enhancing the mobility of the PTMO chains so that they are now able to crystallize in the appropriate temperature range. This result indicates that treatment with base has deencapsulated some of the chains from the surrounding silicate. Also the modulus at room temperature and above is lower by almost an order of magnitude clearly implying a reduced stiffness of the PTMO rich matrix.

Figure 9 shows that the residual weight by TGA of sample B1 is much lower than sample A. In fact, as shown in Figure 10, the residual weight of sample B1 is only slightly more than a sample of endcapped PTMO which has no added TEOS. The PTMO sample shows a residual weight because it is endcapped with siloxy groups which contribute to the residual weight after pyrolysis. Above 700 °C only the silica and other inorganic substances would be expected to contribute to the residual weight, implying that in sample B1 there is almost no silica left in the pyrolyzed film. It is apparent that the base has diffused into the film and solubilized the silicon oxide in the matrix and certainly most of the silicon oxide in the domains. The solubilized product then leaches out of the film leaving the film with a higher organic concentration. Surprisingly sample E has a higher residual weight than sample A. This could possibly be attributed to the sodium that may have precipitated as sodium metasilicate from the saturated solution of NaOH in 2-propanol; however, no analysis was undertaken to prove or disapprove this conjecture. Sample B1 when later immersed in tetrahydrofuran (THF), a good solvent for PTMO, for 48 h to test its mechanical stability did not dissolve, which implied that sufficient network structure is retained. Sample A was also immersed in 1 M NaOH for *over 6 days* with the object of examining its mechanical stability. No appreciable change in the mechanical stability was noticed other than what was noticed in the film that was immersed for 1 day.

Figure 11 shows the ^{29}Si NMR spectrum of samples A and B1. The peaks between ca. −45 and −65 ppm are assigned to the trifunctional silicon species (T), the species attached to the ends of the PTMO chain), while the peaks between ca. −100 and −110 ppm are assigned to the tetrafunctional silicon (Q) species such as in TEOS.[27,28] The superscripts denote the number of −O−

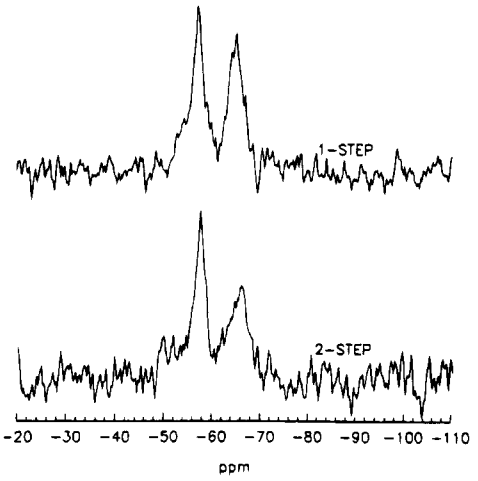

Figure 12. ^{29}Si solid-state MAS NMR of TEOS (0)-PTMO hybrids before and after base treatment denoted by "1-step" and "2-step" spectra respectively.

Si species attached to that particular Si atom; e.g., T^1 implies one −O−Si species attached to the trifunctional silicon atom. For sample A, the trifunctional species are predominantly in the fully condensed (T^3) stage and partially condensed (T^2) stage. The NMR data show that the tetrafunctional silane species is also in the well-condensed (Q^3 and Q^4) stage. In contrast, sample B1 shows no trace of the Q peaks, again supporting the TGA findings that very little of the silicon oxide is present in sample B1. Another observation is that the trifunctional species have partly undergone the reverse condensation reaction showing some T^0 and T^1 peaks. It is speculated that some of the trifunctional species were previously linked with the tetrafunctional species in the acid-catalyzed species. With the dissolution of the silica in the basic medium many of these bonds are broken and show up as the T^0 and T^1 species. Figure 12 shows two NMR spectra—one being a hybrid PTMO network containing no additional TEOS (one step), while the second is of the same network after a base treatment (two step). Here it is seen that the base has not succeeded in hydrolyzing the network structure, i.e., the T^2 and T^3 species are both present in the acid- and base-treated samples which supports the authors speculation that part of the silica in sample A is chemically bonded with the endcapped oligomer.

Figure 13 shows the effect of base treatment on the stress−strain properties of the hybrid materials determined at ambient conditions. The base treatment greatly decreases the modulus of the film and reduces its ultimate elongation. The reduction in the modulus can be explained by a loss of the silica which acts as a reinforcing filler. However, the reduction in ultimate elongation is harder to explain. Both films were extracted in a soxhlet apparatus for 48 h in THF to determine sol content. The sol content of sample A was 1.28%, while that of sample B1 was also very low (1.76%). The low sol content for both films suggested that almost all the organic chains were connected to the network. Swelling in THF for 24 h after extraction resulted in an average increase in weight of 23% for sample A and 107% for sample B1. These results

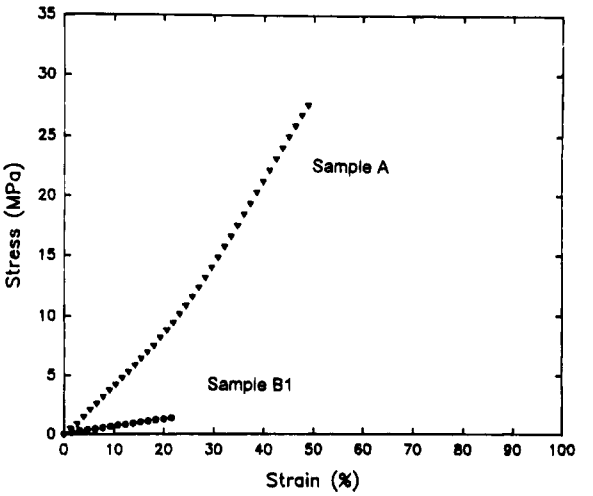

Figure 13. Stress−strain plots of samples A and B1.

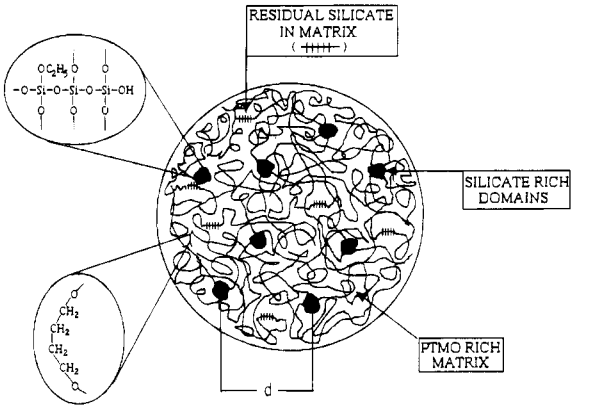

Figure 14. Proposed microstructure of TEOS−PTMO hybrid after 1 M NaOH treatment.

support the ^{29}Si NMR data that show that sample B1 has an "apparently" lower cross-link density. It must be noted that the lower filler content in sample B1 is also significantly responsible for the apparently lower cross-link density. From the above observations it is tentatively concluded that the lower elongation may be due to a larger number of dangling ends in sample B1.

Figure 14 shows the proposed microstructural model of sample B1. The oligomeric matrix is relatively free from silica, and as a result the domains (shown exaggerated in the figure) are better defined. The general periodicity of the domains is maintained.

PTMO/TIOPR Materials. In contrast to the PTMO/TEOS system where the solubility of the metal oxide species is large, the titania-based systems exhibit very low solubility and are investigated here for the purpose of contrasting the effects of varying solubility of the metal oxide phase on the microstructure of the resulting hybrid. The PTMO/TIOPR hybrid materials were also subjected to the base-catalyzed aging process. Figure 15 shows the SAXS profile of sample G (acid-catalyzed sample) and sample H (acid + base catalyzed sample). The gradual decrease in the intensity beyond the peak at higher values of s suggests a fairly mixed inorganic−organic system. In great contrast, the SAXS profile of sample H shows a strong increase in peak intensity. The peak is much sharper, and the precipitous drop in intensity beyond the main peak supports the idea of a sharper phase-separated system. The invariant of the curves is given by the formula

(27) Marsman, H. *NMR Oxygen-17 and Silicon-29*; Diehl, P., Fluck, E., Kosfield, R., Eds.; Springer-Verlag: Berlin: Vol. 17.
(28) Sindorf, D. W.; Maciel, G. E. *J. Am. Chem. Soc.* **1983**, *105*, 3767−3776.

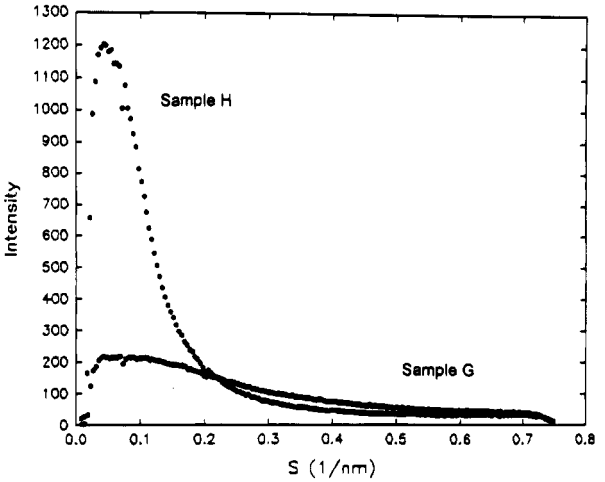

Figure 15. SAXS profiles of samples G and H.

$$Q = \int I(s)s \, ds \tag{6}$$

where $I(s)$ is the slit-smeared intensity and s is as defined earlier. Both curves taper to almost identical values of intensity at higher s values. However, the slightly higher intensity values at the intermediate s values for sample G is more than compensated for by the contribution of sample H to the intensity at the lower values of s, and this makes the value of the invariant higher in sample H. Numerical calculations show that the ratio of the invariant for sample A to that of sample B in 1:1.11. For a system with the same volume fractions and assuming no change in the electron density of the phases, the invariant is proportional to the degree of phase separation or sharpness of the boundary between the phases. Another way of visualizing the change is by considering the following equation for the mean-square electron density difference of the system which is proportional to the invariant for an ideally sharp interface. Any deviation from ideality such as mixing at the interface lowers the electron density difference and the resulting integrated scattering intensity:

$$\langle \Delta\varrho^2 \rangle \propto \phi_1\phi_2(\varrho_1 - \varrho_2)^2 \tag{7}$$

where $\langle \Delta\varrho^2 \rangle$ is the value of the mean square of the electron density fluctuation; ϱ_1 and ϱ_2 are electron densities of phase 1 and 2 respectively; ϕ_1 and ϕ_2 are volume fractions of phase 1 and 2, respectively. If the volume fractions are unchanged, the difference in the electron density would have to be increased to account for the higher intensity. Brennan[29] has shown that the SAXS peak intensity of a TIOPR/polyimide hybrid network as well as in some other hybrids increased steadily with an increase in the curing temperature which ranged from 150 to 325 °C. This was attributed to the higher extent of reaction at the higher temperature which increased the average electron density of the inorganic domains. Aging processes can also lead to densification by dissolution and reprecipitation of the inorganic oxide. In the case of PTMO/TEOS, the high solubility of silica in the alkaline solution precluded densification. By contrast, in the PTMO/TIOPR system the low solubility of titania in the alkaline solution forces it to remain in the hybrid network. Thus, both densification and phase separation occurs as a result of aging and lead to a higher SAXS intensity. Figure 15 shows that the interdomain distance has also increased slightly which again supports the conclusion that the aging has resulted in a redistribution of the titania.

(29) Brennan, A. B. Ph.D. Thesis, VPI & SU, Materials Engineering Science Program, 1990.

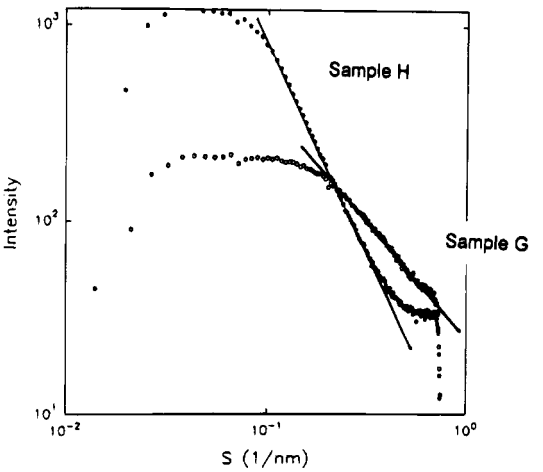

Figure 16. SAXS profiles of samples G and H on a double logarithmic scale.

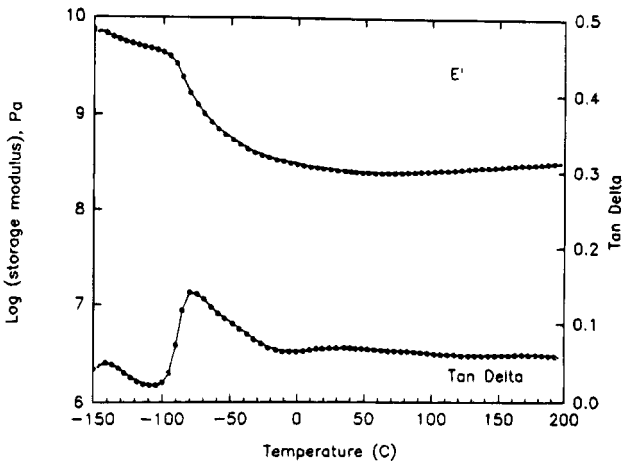

Figure 17. Storage modulus and tan δ versus temperature for sample G.

Figure 16 shows the curves in Figure 15 drawn on a log–log plot (Porod plot). The Porod plot clearly highlights the densification of the titania domains. The plot shows that the absolute value of the slope of sample H is 3.10 and is much larger than that of sample G, which is 2.13. The smaller absolute value of the slope, as has been mentioned before is a measure of the openness of the inorganic domain with a larger absolute value corresponding to a less-open and more ramified domain.

The effects of densification on the mechanical properties were evaluated by dynamic mechanical analysis. Figure 17 shows the dynamic mechanical plot of the acid-catalyzed PTMO/TIOPR system (sample G). The plot shows a transition at around −120 °C which is attributed to the crankshaft motion of the methylene units as mentioned earlier. The transition at −80 °C is due to the relaxation of the PTMO chains. The transition is broad and suggests that a variety of molecular environments is present around the PTMO chains. It must be noted that the titanium-based materials give a less broad transition than that by the

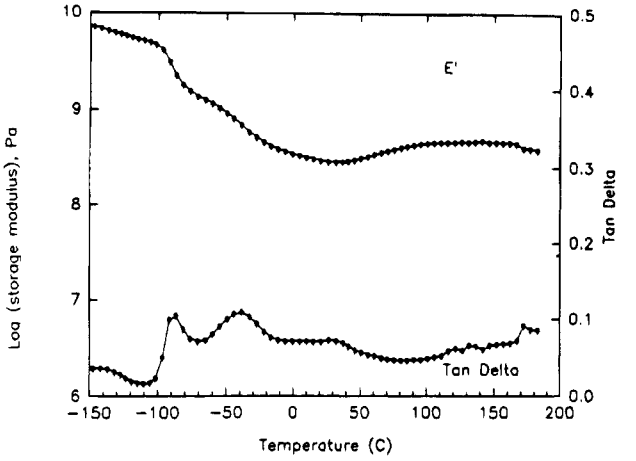

Figure 18. Storage modulus and tan δ versus temperature for sample H.

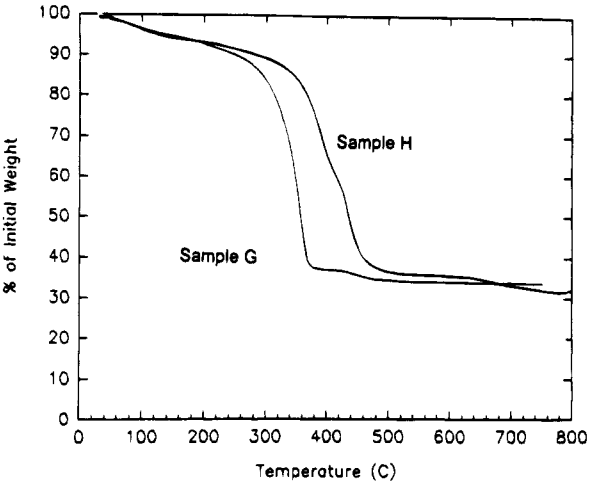

Figure 19. TGA profiles of samples G and H.

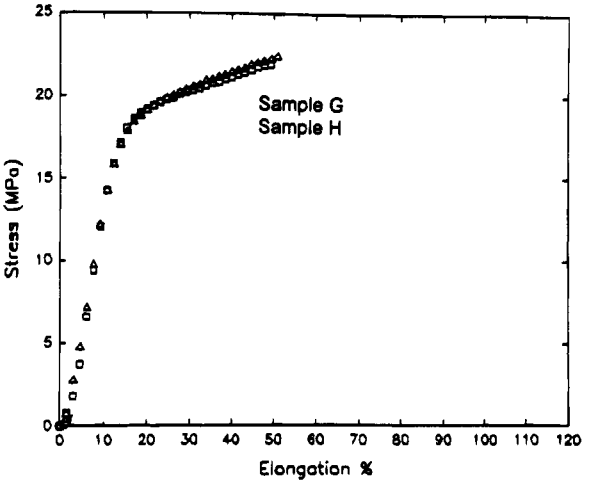

Figure 20. Stress–strain plots of samples G and H.

TEOS materials, implying more pure PTMO environment in the titanium-based hybrids. This difference has been observed elsewhere[8,29] and has been attributed to the tendency of the titanium alkoxide to react with itself due to its higher reactivity as compared to the silicon alkoxide. During the transition, the varied environments hinder the relaxation of PTMO by various degrees. No evidence of a crystalline peak is seen in the tan δ spectrum implying that the hindrance to mobility is large enough to prevent crystallization of the PTMO chains. The modulus at room temperature and above is between 10^8 and 10^9 Pa, typical of a partially cross-linked elastomeric network.

Figure 18 shows the DMA profile of the base-treated hybrid film. The transition at −120 °C is again present. Whatever the effects on morphology, this transition remains unaffected. The crankshaft motion of the methylene chains occurs over a length scale of approximately 6–7 Å (4 × 1.54 Å), while the molecular motions occurring at higher temperatures such as the glass transition occur at length scales at least a magnitude higher. The fact that this transition is unaffected implies that the changes in morphology do not affect the local mobility of the tetramethylene units. In contrast, the glass transition has shifted to a lower temperature if the temperature at the peak in the tan δ spectrum is taken as the glass transition temperature. At the transition, the storage modulus decreases; however, the rate of decrease of the storage modulus slows at approximately −50 °C, which coincides with the onset of the second peak. The second peak has a maximum at ca. −35 °C. As in the TEOS/PTMO base-treated system, this peak is again attributed to the melting of the PTMO crystallites, as has been proven in the PTMO/TEOS system. The shift in the glass transition dispersion to a lower temperature and the transient crystallinity observed above the T_g temperature distinctly and strongly support the notion that the PTMO chains have greater mobility in the base-treated film (sample H) and that the PTMO chains are better phase separated and have less hindrance to their movement. The modulus at room temperature and above is comparable to the acid-catalyzed film. There is a slight increase in modulus above ca. room temperature probably due to the condensation of some of the hydrolyzed titanium and the triethoxysilicon species. This is in contrast to the PTMO/TEOS system where for the base-treated film (sample B1), a large decrease in modulus of almost an order of magnitude was observed. *Clearly the network cross-link density of the PTMO/TIOPR system is unaffected by the alkaline treatment.*

It may be recalled that the loss in network cross-link density was attributed to the loss of silica in the PTMO/TEOS system, which was supported by a TGA analysis. A similar TGA analysis was done for samples G and H and is shown in Figure 19. Both samples have almost *identical residual weights*. This implies that the titania, not surprisingly, is negligibly soluble in 1 M NaOH because of the low solubility of the titania in dilute aqueous solutions. There is no net loss of filler, and so the apparent cross-link density is maintained. Thus, the higher intensity of sample H in the SAXS profile of the PTMO/TIOPR system, as compared to the PTMO/TEOS system, can be principally attributed to (1) higher electron density difference between inorganic domains and matrix and (2) higher inorganic content in sample H, although part of the intensity difference may be reduced by the sharper phase separation in the PTMO/TEOS system.

Figure 20 shows the stress–strain data for the TIOPR/PTMO system. The initial Young's modulus and the final elongation coincide with the acid-catalyzed film. The figure shows that the higher phase separation and the densification do not significantly affect the mechanical tensile properties unlike in the PTMO/TEOS system. These results agree with those obtained from DMA data at ambient conditions which show essentially

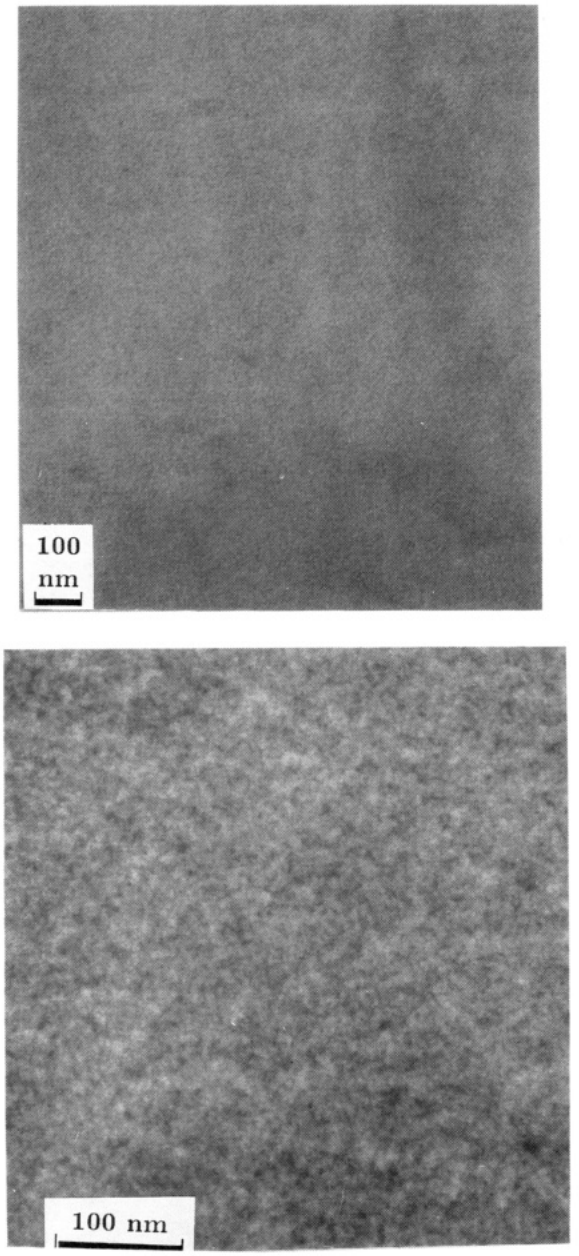

Figure 21. (A) Transmission electron micrograph of sample G. (B) Transmission electron micrograph of sample H.

no difference in the magnitude of the storage modulus between the acid- and base-treated samples. The tensile data indirectly show that the network cross-link density remains intact in the presence of titanium oxide. Thus cross-linking in the presence of titania may be one method of imparting chemical stability to the network with respect to the alkaline environment.

Finally, a transmission electron microscopy study was conducted in an attempt to corroborate the conclusions about the microstructure which were derived from SAXS and other analysis. Figure 21A shows a TEM micrograph of the acid-catalyzed sample. The micrograph shows a uniform morphology with a microstructure that is not distinct which could be due to the insufficient density difference between the inorganic and the organic domains. Figure 21B, however, shows a TEM micrograph of the base-treated film. While high detail is lacking due to domain overlap as well as size variations, clearly a texture is seen which is composed of domains in a matrix. The thickness of the sample and the domain concentration [domains/unit volume] prevent determination of the individual domain size, but a circular cross section is seen for the microstructure. The microstructure is in qualitative agreement with the model originally proposed by Huang.[13]

Summary and Conclusions

Aging of a PTMO/TEOS hybrid in 1 M NaOH for 24 h results in a better-defined two-phase microstructure. The matrix which is composed mostly of the oligomer is more homogeneous, and the domains which are mostly silicon oxide are more densified. TGA analysis showed that the residual weight of the base-treated sample had a lower silicon oxide content than the untreated sample which was expected due to the solubility of silicon oxide in highly basic solutions. Dynamic mechanical analysis showed that the aged hybrid exhibited better chain mobility, which resulted in a shift of the glass transition temperature of the oligomeric phase to a lower temperature and an ability to undergo crystallization. The apparent cross-link density was lower partly due to the lower silicon oxide content and in part due to decondensation of the triethoxysilane cross-linked PTMO network. This resulted in a decrease in the modulus of the aged hybrid. The removal of the silicon oxide from the matrix was dictated by its solubility in the aging solution. The solubility of the silicon oxide and the affinity of the organic matrix determined the resulting microstructure of the aged hybrid. These results also support the microstructural model originally proposed for the hybrid materials.

In PTMO/TIOPR hybrids, due to the lower solubility of titanium oxide in 1 M NaOH solutions, the aging treatment resulted in a hybrid where the inorganic content was little changed. However, base treatment resulted in better phase separation between the inorganic and the organic phases as in the PTMO/TEOS hybrid. As a result of the enhanced phase separation, the mobility of the organic phase was increased which resulted in a lowering of the glass transition temperature and also crystallization of the PTMO chains. The initial modulus and the ultimate elongation were unchanged. TEM data qualitatively agree with the originally proposed microstructural model of the hybrid materials. The above results show that the aging process offers another route towards modifying the microstructure of hybrid materials.

Acknowledgment. Financial assistance from the Office of Naval Research is gratefully acknowledged.

CM940448X